JOURNAL OF AIRCRAFT
Vol. 46, No. 2, March–April 2009

Conceptual Design Considerations for Microwave- and Solar-Powered Fuel-Less Aircraft

Adam M. Wickenheiser* and Ephrahim Garcia†
Cornell University, Ithaca, New York 14850

DOI: 10.2514/1.37669

Unmanned aerial vehicles typically have limited flight duration, particularly at smaller scales. A microwave-/solar-powered flight vehicle, on the other hand, can remain in theater continuously by harvesting electromagnetic radiation using onboard antennas and solar panels. Moreover, these seemingly disparate power sources are complementary in that they are both heavily dependent on the wing area. Rectifying antennas are used to harvest power and convert it into electrical energy usable by the onboard motors and other electronics. To supplement this energy source, photovoltaic cells are used to harness incoming solar radiation. Discussed herein are design features of fuel-less air vehicles and their sensitivity to several key performance metrics for this class of aircraft. In this study, aircraft with wingspans in the range 3–5 m and cruise $Re = 5 \times 10^5$–5×10^6 are considered. New metrics are presented that are unique to a microwave-powered aircraft and are useful in the development of its missions. These metrics relate the design of the aircraft and the energy transmitter to the duration and range of the vehicle's missions. The addition of solar power harvesting to a microwave-powered aircraft is examined. Furthermore, an examination of the strong coupling among the aircraft's flight performance, power harvesting abilities, and its mission capabilities is given. Traditional and nontraditional wing shapes are presented to motivate a discussion of this coupling. In particular, tradeoffs between flight performance and power harvesting performance are discussed.

Nomenclature

A	=	actual patch area
A_{eff}	=	effective patch area
A_{tr}	=	transmitter dish area
AR	=	aspect ratio
b	=	wing span
C_{D_0}	=	parasite drag coefficient
C_f	=	flat-plate skin friction drag coefficient
$\bar{c}$	=	mean aerodynamic chord
D	=	drag force magnitude
d	=	fuselage diameter
E	=	stored energy
E_{cap}	=	energy storage capacity
E_{solar}	=	incident solar irradiance
FF	=	component form factor
f	=	microwave frequency
G_{dir}	=	microwave transmitter directivity loss
G_{tr}	=	microwave transmitter gain
h	=	altitude
L	=	lift force magnitude
l	=	fuselage length
l_t	=	distance between wing and tail quarter-chord lines
P_{patch}	=	received microwave power at a patch
P_{req}	=	power required for flight
P_{solar}	=	received solar power
P_{tr}	=	microwave transmitter power
$P_{\mu w}$	=	received microwave power
Q_{int}	=	component interference factor
R	=	flight range
r	=	distance from microwave transmitter to aircraft
r_{eq}	=	equilibrium power radius
r_{nr}	=	no-return radius
r_{tr}	=	microwave transmitter dish radius
S	=	wing planform/reference area
S_{wet}	=	wetted area
T	=	thrust magnitude
t/c	=	thickness-to-chord ratio
t_{loiter}	=	loiter time at a given distance
V	=	cruise velocity
W_{pay}	=	payload weight
W_{struct}	=	aircraft structural weight
W_0	=	aircraft gross weight
α	=	angle of attack
η_{airfoil}	=	wing airfoil efficiency
η_{m+p}	=	motor/propeller efficiency
η_{pv}	=	photovoltaic cell efficiency
η_r	=	rectenna efficiency
η_{tr}	=	microwave transmitter efficiency
θ	=	angle between patch normal and microwave beam direction
Λ	=	sweep angle
λ	=	microwave wavelength
ϕ	=	angle from transmitter boresight

Received 21 March 2008; revision received 6 November 2008; accepted for publication 12 January 2009.

*Postdoctoral Associate, Sibley School of Mechanical and Aerospace Engineering, 214 Upson Hall. Student Member AIAA.

†Associate Professor, Sibley School of Mechanical and Aerospace Engineering, 224 Upson Hall. Member AIAA.

I. Introduction

WIRELESS power transmission through electromagnetic wave propagation began with the pioneering work of Heinrich Hertz and was made famous by the spectacular demonstrations of Nicola Tesla; however, practical methods of focusing and directing high-power electromagnetic energy have only existed since the 1930s. Furthermore, efficient means for converting this energy into usable direct current at appreciable power densities did not exist before the development of the rectenna (or rectifying antenna) in the 1960s. The development of this invention and the desire to communicate by line of sight over large distances subsequently spurred research in the area of fuel-less aircraft [1].

An aircraft that harvests energy from solar and microwave sources has the potential for extremely long persistence in its theater of operation. Aircraft powered by solar energy alone have garnered a significant amount of research since the 1980s for use in extremely long-duration missions, including several successful aircraft developed by AeroVironment. (See [2] for an extensive list of

citations.) Although, in the case of aircraft powered by microwave energy alone, the overall system is energy inefficient due to the fact that only a small portion of the transmitted power is captured by the aircraft; the promise of persistent high-altitude communications and surveillance has nevertheless attracted significant study over the past 50 years. Landmark experiments on microwave-powered airborne platforms were conducted by Brown on a tethered helicopter platform [3] and by DeLaurier et al. on a free-flying, fixed-wing aircraft [4]. Both of these experiments used large external rectenna arrays that were not integrated into the geometry of the aircraft. Microscale and flexible rectennas [5,6], however, provide a solution to integrate the antenna into the structure of the airframe as well as conform it to its aerodynamic surfaces. This integration of energy harvesting elements presents a more efficient solution to the fuel-less aircraft design problem by not sacrificing aerodynamic performance.

One of the goals of this study is to present several new aircraft performance metrics that arise from the unique constraints placed on microwave-powered aircraft. Numerous aspects of aircraft design, mission profile, and trajectory optimization have been studied for this class of air vehicle. The feasibility of several microwave-powered aircraft designs has been considered along with the designs' sensitivity to variations in geometry, mission parameters, and ground transmitter capabilities [7–10]. Other studies have looked into trajectory optimization for stationkeeping over the power source in the presence of wind or measurement uncertainty [11–13]. These studies, however, do not investigate the coupling between the aerodynamic performance and the energy harvesting performance. Indeed, the wing shape and size can be designed to strike an optimal balance between aerodynamics and harvesting capabilities. Furthermore, the mission profile has a large impact on the optimal design. For example, an aircraft design for perpetual stationkeeping over the microwave transmitter will not have the same aerodynamic capabilities as a long-range surveillance aircraft.

This paper focuses on several of the key metrics to consider when designing a fuel-less aircraft and its mission profile, some of which were previously discussed in [14]. These include traditional measures, such as endurance, range, and required power, and several new metrics, such as equilibrium power radius, that describe the aircraft's capabilities as a function of the distance from the transmitting power source. The sensitivity of each of these metrics to design parameters and the physical basis for maximizing them is presented. Although a detailed study of design aspects for solar-powered aircraft is beyond the scope of this effort, the impact of solar power harvesting in conjunction with microwave power harvesting is examined using a simplified solar energy model. Finally, the coupling between power harvesting and aerodynamics and its impact on flight performance is discussed.

II. Modeling Description and Performance Evaluation Methodology

A. Aircraft Model

To evaluate the mission performance of a fuel-less aircraft, an accurate model of the aircraft's relevant parameters, including aerodynamics, weights, and geometric layout, is needed. This will enable a simultaneous calculation of its flight performance and energy harvesting capabilities, which is necessary when estimating the aircraft's overall effectiveness as a fuel-less reconnaissance flight vehicle. For this study, only the dynamics of the aircraft on the time scale of the mission are studied; therefore, the transient dynamics of the vehicle and flowfield are ignored. Lateral terms such as turning radius are also not considered because they are insignificant compared to the mission-level length scales studied in this work. Thus, the aircraft is modeled in steady-state straight-and-level flight; that is, only the trim lift and drag forces are computed for a given angle of attack. It is assumed that all moments are balanced, and so rotational dynamics are not considered. The steady-state equations of motion for the aircraft in straight-and-level flight are

$$T\cos\alpha - D = 0 \tag{1}$$

$$-T\sin\alpha + L - W_0 = 0 \tag{2}$$

where it is assumed that the thrust vector is aligned with the aircraft.

This study focuses only on the impacts of design parameters relevant to the aircraft's sizing and wing geometry; therefore, other geometrical parameters, such as those pertaining to layout, tail sizing, and fuselage fineness, for example, are specified as constants. These parameters are listed for a baseline design in Table 1. They are the result of iterations on previous microwave-powered aircraft designs [15], and, where dimensions are not provided in the literature, the conceptual design approach outlined in [16] is used for aircraft sizing. When the aircraft is scaled to meet mission or payload requirements, as outlined in Sec. II.D, all of these parameters are scaled together.

The lift and induced drag forces on the wing are computed using a modified version of Weissinger's method that has been developed specifically for nontraditional wing shapes [17]. This method is based on the lifting-line theory; therefore, it is only valid when the flow can be approximated by potential theory. Nevertheless, this does not present a major limitation because this study only considers subsonic flight at angles of attack at which the flow remains attached. The output of this method is a one-dimensional lookup table that provides the lift and induced drag forces on the wing as a function of angle of attack. The three wing shapes under consideration in this study are depicted in Fig. 1 with the dimensions listed in Table 1, and their respective drag polars are given in Fig. 2. It is assumed that all three wings have a constant airfoil section along the entire span, and the airfoil's efficiency is 90% that of the theoretical low-speed lift slope of 2π. The rectangular and elliptic wings are presented as baseline designs, whereas the bulbous wing is offered as an improved design for microwave energy transmission. This wing features a large, circular inboard section to present an ideal target for microwave power reception, and the wingtips are reduced in chord length to maintain a high aspect ratio. The elliptic wing possesses the highest lift-to-drag ratio, as predicted by lifting-line theory [18]. The bulbous wing is the least efficient at this aspect ratio because of the large downwash over the center section due to the effective forward sweep of the wings. The rectangular wing falls between the other two in terms of aerodynamic efficiency.

Because potential flows are assumed, these forces scale proportionally with the square of velocity. Although this method provides an estimate of induced drag, the parasite drag must be calculated separately. In this study, the method used for calculating parasite drag is the component buildup method summarized by Eq. (3), provided by [19],

$$C_{D_0} = \frac{\sum (C_f F F Q_{\text{int}} S_{\text{wet}})}{S} \tag{3}$$

Thus, an estimate of the parasite drag is given by the sum of each component's contribution, scaled by an interference factor and normalized by the wing area. Empirical equations for these terms are given in [19]. (In this study, leakage, protuberance, and miscellaneous drags are ignored.)

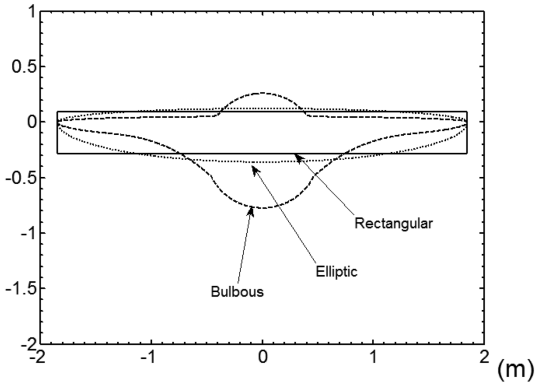

Fig. 1 Wing planforms under consideration, $AR = 10$.

Table 1 Baseline aircraft geometry parameters

Fuselage:			
d	Diameter	0.50	m
l	Length	4.50	m
l_t	Wing-to-tail-distance	2.90	m
Wing:			
b	Span (tip to tip)	3.70	m
S	Planform area	1.40	m^2
t/c	Thickness-to-chord ratio	0.1	
η_{airfoil}	Airfoil efficiency	0.90	
Horizontal tail:			
S	Planform area	0.09	m^2
$\bar{c}$	Mean aerodynamic chord	0.07	m
Λ	Sweep angle	10	deg
t/c	Thickness-to-chord ratio	0.1	
Vertical tail:			
S	Planform area	0.04	m^2
$\bar{c}$	Mean aerodynamic chord	0.03	m
Λ	Sweep angle	15	deg
t/c	Thickness-to-chord ratio	0.1	

An accurate weights model is also necessary to model the mission performance of the aircraft accurately. For instance, the weight penalty for a larger or higher aspect ratio wing must be considered to converge on a feasible design. The model used herein is based off of empirical equations given in [20], which give the variations in structural weight as size, layout, and planform geometry vary. It is also assumed that the electric motor constitutes 8% of the gross weight of the aircraft. This percentage is inferred from existing data on large-scale, electric-powered model aircraft [21].

B. Power Harvesting System Model

The fuel-less aircraft under consideration is powered by both microwave and solar radiation, and excess energy is stored in onboard batteries. Furthermore, it is assumed that the entire wing surface is used for energy harvesting: the upper surface is covered in photovoltaic cells, and the lower surface is covered in rectifying patch antennas (or rectennas). The microwave ground transmitter is modeled as a parabolic dish whose gain is varied in this study. Representative values for the energy harvesting system's parameters are given in Table 2.

The incident solar radiation E_{solar} listed in Table 2 is the midpoint of the clear-day, direct solar radiation and the cloudy-day, diffuse solar radiation design envelopes given by [23]. This value gives a measure of the average impact of solar power harvesting over the length of an entire day (when the sun is out) and across all visibility conditions. If a more specific sunlight condition is desired, a different value for E_{solar} may be substituted into the model derived below. The value is further reduced by a factor of 10% to account for the

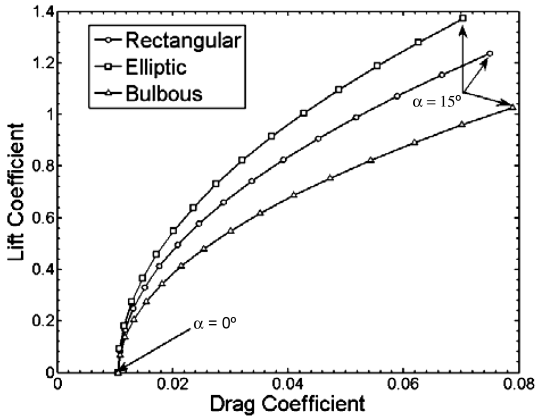

Fig. 2 Drag polars of various wing planforms, $AR = 10$, $\alpha = 0$–15 deg.

Table 2 Energy harvesting system parameters

Solar:			
η_{pv}	Photovoltaic cell efficiency [22]	0.18	
E_{solar}	Incident solar irradiance [23]	570	W/m^2
Microwave:			
f	Frequency	5.8	GHz
P_{tr}	Transmitter power	1.0	MW
η_{tr}	Transmitter efficiency	0.55	
r_{tr}	Transmitter dish radius	3.5	M
G_{tr}	Transmitter gain	60	dB
η_r	Rectenna efficiency [24]	0.60	
Storage:			
E_{cap}	Battery storage capacity	1.15	MJ
W_{battery}	Battery weight	2.0	kg
Output:			
η_{m+p}	Motor/propeller efficiency [21]	0.56	

curvature of the upper wing surface. This factor is computed by integrating the incidence angle of the upper surface of a NACA 0012 airfoil, used in previous microwave aircraft designs [12], and rounding up for conservatism. Thus, the power gathered from the solar cells is approximated by

$$P_{\text{solar}} = \eta_{\text{pv}} E_{\text{solar}} S \cos\alpha \tag{4}$$

where it is assumed that the incident radiation comes from directly overhead. (Note that the effects of the solar incidence angle are built into the value of E_{solar}.)

The power received by the aircraft from beamed microwave radiation is similar in nature to the power received by solar radiation but further complicated by the nonuniformity of the incoming waves. The power received by an infinitesimal rectenna patch is given by

$$\mathrm{d}P_{\mu w} = \eta_r \frac{P_{\text{patch}}}{4\pi r^2} \mathrm{d}A_{\text{eff}} \tag{5}$$

where the term $P_{\text{patch}}/(4\pi r^2)$ is analogous to E_{solar} in Eq. (4) and represents the microwave irradiance at each patch. This term varies over the wing planform as a function of the angle of incidence between the surface and the incoming wave and the distance from the boresight of the transmitter. The rectenna efficiency η_r is a combination of the power conversion efficiency and the patch layout efficiency. It is assumed that the microwave radiation and rectenna layout are circularly polarized, meaning that the incoming microwave beam may be rotated about its axis of symmetry without affecting the power received by the rectenna. The effective area of each patch element can be approximated by

$$\mathrm{d}A_{\text{eff}} = \cos^2\theta \, \mathrm{d}A \tag{6}$$

This equation takes into account the reduction in projected area and the reduction in rectenna gain as the angle of the incoming radiation is reduced from perpendicular.

Microwave power is beamed to the aircraft from a stationary ground transmitter modeled as a simple parabolic dish, whose gain along the boresight is given by

$$G_{\text{tr}} = \frac{\eta_{\text{tr}} 4\pi A_{\text{tr}}}{\lambda^2} \tag{7}$$

The transmitter's directivity results in a decrease in this gain as the angle from the boresight increases. Thus, only the element of the patch antenna directly along the boresight of the transmitter dish receives the gain in power given by Eq. (7); all other patches experience a loss given by

$$G_{\text{dir}} = \left(\frac{J_1\left(\frac{2\pi r_{\text{tr}}}{\lambda} \sin\phi\right)}{\frac{2\pi r_{\text{tr}}}{\lambda} \sin\phi} \right)^2 \tag{8}$$

where $J_1(\cdot)$ is a first-order Bessel function of the first kind [25]. Thus,

the received microwave power at each patch is given by

$$P_{\text{patch}} = G_{\text{tr}} G_{\text{dir}} P_{\text{tr}} \tag{9}$$

Substituting Eqs. (6–9) into Eq. (5) and integrating over the entire wing planform gives the total usable microwave power

$$P_{\mu w} = \int_S \frac{\eta_r G_t G_{\text{dir}} P_t \cos^2\theta}{4\pi r^2} \mathrm{d}A \tag{10}$$

The total power received from both sources is therefore the sum of Eqs. (4) and (10).

C. Performance Evaluation

Several metrics are presented herein as a means by which the performance of a fuel-less aircraft can be evaluated. These metrics represent independent axes in the design space for this type of aircraft, whereby a particular aircraft may be designed as a compromise among various performance criteria. For example, depending on the mission for which the aircraft is designed, either long range or long endurance might be preferred, or a compromise therein. In Sec. III, a maximization (or minimization) of each metric presented here is sought, independent of the other metrics, and the differences in each design are discussed.

The first and most straightforward metric to be discussed is the power required for straight-and-level flight. It is given simply by

$$P_{\text{req}} = \frac{TV}{\eta_{m+p}} \tag{11}$$

that is, the product of thrust and cruise velocity, divided by the motor and propeller efficiencies. Minimizing the power required for flight means less average power needs to be harvested, which in turn reduces the wing size and power conversion efficiency requirements as governed by Eqs. (4) and (10). A reduction in power consumed also means that, for a given transmitter power, the aircraft can be farther away from the ground station and still receive enough average power to maintain altitude. Alternatively, the transmitter may be switched off for longer periods of time or pulsed at a lower duty cycle while the aircraft runs on battery power. Minimizing the required power for flight equates to maximizing the loiter endurance of the aircraft. Thus, the aircraft can loiter for longer periods of time when it is outside the effective range of the ground transmitter and receiving inadequate power from microwave and solar sources.

Another metric considered in this study is the equilibrium power radius r_{eq}, the radius at which the power required for flight equals the power received from solar and microwave energy. This radius demarcates the boundary of a "safe zone" inside which the aircraft can loiter indefinitely and/or recharge its batteries, assuming the transmitter remains on and the solar irradiance remains constant. Outside this radius, the power required for flight exceeds the power received; therefore, the aircraft must eventually return to within this radius to begin recharging its batteries. To derive a formula for this radius, it is assumed that the microwave beam incidence angle is constant across the entire planform and that there is no loss from the directivity of the transmitter [Eq. (8)], which are reasonable assumptions when the aircraft is far away from the ground station. The equilibrium power condition yields

$$P_{\text{req}} = P_{\mu w} + P_{\text{solar}} = \frac{\eta_r G_{\text{tr}} P_{\text{tr}} S}{4\pi} \frac{(h\cos\alpha - r_{\text{eq}}\sin\alpha)^2}{(r_{\text{eq}}^2 + h^2)^2} + \eta_{\text{pv}} E_{\text{solar}} S \cos\alpha \tag{12}$$

Solving for r_{eq} gives

$$r_{\text{eq}} = \frac{-C_2 \sin\alpha + \sqrt{C_2^2 \sin^2\alpha + 4C_1 C_2 h \cos\alpha - 4C_1^2 h^2}}{2C_1} \tag{13}$$

where

$$C_1 = \sqrt{1 - \frac{\eta_{\text{pv}} E_{\text{solar}} S \cos\alpha}{P_{\text{req}}}} \quad \text{and} \quad C_2 = \sqrt{\frac{\eta_r G_{\text{tr}} P_{\text{tr}} S}{4\pi P_{\text{req}}}} \tag{14}$$

Equations (13) and (14) indicate that r_{eq} varies with angle of attack; r_{eq} is greater if the aircraft is flying toward the transmitter than away from it because in the former case it is exposing a larger projected area to the incoming microwave beam. Additionally, r_{eq} increases as P_{solar} [Eq. (4)] increases and becomes infinite when $P_{\text{solar}} = P_{\text{req}}$. These equations also indicate that the ratio S/P_{req} must be maximized to maximize r_{eq} at a given angle of attack.

Range is another important metric for describing the performance of a surveillance aircraft because it determines how much ground area can be surveyed using a given amount of stored energy. Range is given by the formula

$$R = E_{\text{cap}} \frac{V}{P_{\text{req}}} \tag{15}$$

for a battery-powered aircraft. Thus, maximizing the range equates to maximizing the ratio V/P_{req}, for a given energy storage capacity.

Closely related to this metric, in the case of fuel-less aircraft, is the concept of no-return radius r_{nr}. The no-return radius is the distance from the transmitter at which the aircraft must turn around and return to the equilibrium power radius or sacrifice altitude. It also represents the distance at which approximately half the aircraft's stored energy, plus the energy it harvested on the way out, is expended. To calculate r_{nr}, it is assumed that the aircraft's batteries are fully charged when it leaves the region bounded by the equilibrium power radius r_{eq}. During its flight outside r_{eq}, the aircraft's stored energy dynamics are governed by

$$\dot{E} = P_{\mu w} + P_{\text{solar}} - P_{\text{req}} \tag{16}$$

The no-return radius is the radius at which it must turn around to reach power equilibrium again before running out of stored energy, as depicted in Fig. 3. Note that the equilibrium radius on the return trip $r_{\text{eq,back}}$ is outside the equilibrium radius for the outgoing leg $r_{\text{eq,out}}$ because the aircraft exposes more of its lower surface to the transmitter on the way back, as mentioned previously. Although there is no simple expression for r_{nr}, it increases with increasing cruise velocity and wing planform area and decreases with increasing P_{req}. Considering that received microwave energy is negligible at large distances from the transmitter, the no-return radius is roughly half the range given by Eq. (15). This is also demonstrated by the approximately linear decay in stored energy as the aircraft flies outside the equilibrium power radius, shown in Fig. 3.

Similar to the calculation of the no-return radius is the evaluation of the time the aircraft can spend at a given distance from the transmitter. Clearly, this time is infinite inside the equilibrium power

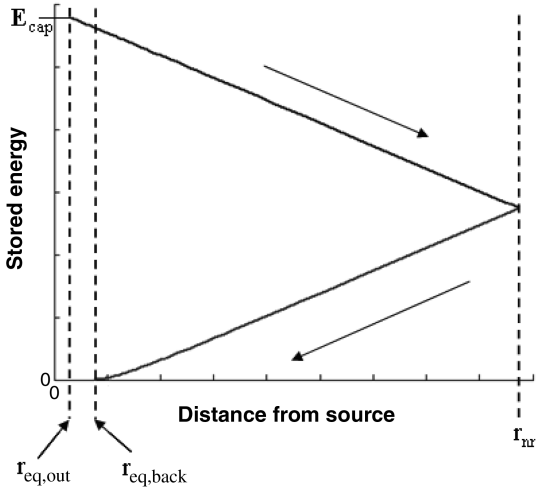

Fig. 3 Energy consumption during flight to and from r_{nr}.

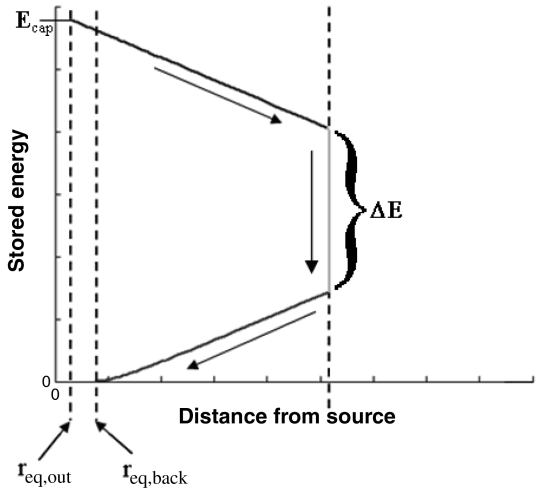

Fig. 4 Energy consumption during loiter outside r_{eq}.

radius and zero at the no-return radius; however, between these radii the stored energy is continually dropping, and so the loiter time assumes a finite value here. To compute the loiter time, first the aircraft power and velocity are integrated out to the desired distance, starting from $r_{eq,out}$ and full battery charge. Simultaneously, the aircraft is integrated backward in time from $r_{eq,back}$ to the same distance to compute the required energy for the return trip. The remaining energy is then used to find the time the aircraft may loiter at that distance, given by

$$t_{\text{loiter}} = \frac{\Delta E}{P_{\text{req}}} \tag{17}$$

where ΔE is depicted in Fig. 4.

D. Optimization Procedure

The goal of the optimization procedure used in this study is to maximize or minimize each of the performance metrics, described in the previous section, by varying the geometry of the aircraft and its equilibrium flight condition, in this case, the trim angle of attack. Because an exhaustive search of the entire design space of a fuel-less aircraft is impractical, this study focuses only on the wing geometry and the overall aircraft sizing. Thus, the relative size and layout of the fuselage and tail components remain fixed, whereas the wing geometry and absolute scale are allowed to vary. This simplification is chosen to reduce the number of optimization variables and to make the sensitivity of each metric to geometry and aerodynamics clear. This procedure is also analogous to the initial sizing procedure used in standard aircraft design [16].

This optimization study considers various wing aspect ratios and shapes, as listed in Table 3. A payload weight of 2 kg and an operating altitude of 1000 m are chosen as fixed design requirements. Angle of attack constraints of 0–15 deg are chosen to limit the flight to fully attached flow regimes, which meet the requirements of the chosen aerodynamic analysis method [17]. A minimum structural weight fraction of 0.6 is chosen based off of historical trends, including previous microwave-powered aircraft designs [10,26]. This fraction is the ratio of structural weight to gross weight, and a minimum bound on this value represents a minimum amount of structure needed to carry the weight and aerodynamic loads during flight. A further constraint is one on minimum flight speed. This speed is tabulated in [23] as the 99% design scalar wind speed envelope, meaning that at any given time there is a 99% probability that the wind speed will be below this value. The minimum speed constraint used in this study is 20% higher than the tabulated envelope for additional conservatism, because flying below this speed makes trajectory tracking and stationkeeping less reliable. These optimization parameters and constraints are summarized in Table 3.

The nonlinear programming method used to solve the optimization problem is sequential quadratic programming [27], which is a gradient-type algorithm that handles nonlinear cost and constraint functions. During each evaluation of the cost function, the weights model must be computed iteratively, because the structural weight is a function of the gross weight and vice versa. Also, the trim equations [Eqs. (1) and (2)] must be solved as a function of angle of attack (one of the optimization variables). To evaluate the no-return radius and loiter time, a fourth- to fifth-order adaptive Runge–Kutta algorithm [28] is used for the integration of the power balance [Eq. (16)].

III. Results

A. Single Configuration Performance Evaluation

The surveillance capabilities of a fuel-less aircraft with a rectangular wing of aspect ratio 10 are analyzed in terms of the performance metrics described in Sec. II.C. Using the optimization procedure described in Sec. II.D, the power required for straight-and-level flight [Eq. (11)] is minimized in terms of angle of attack and aircraft scale. A summary of this configuration's geometry and performance metrics is given in Table 4. These metrics are evaluated for the same configuration with and without solar power harvesting. The results indicate that the presence of solar power has a much smaller impact on the equilibrium power radius compared to the no-return radius. This is due to the fact that microwaves are the dominant source of energy near the transmitter: the relatively small power gained from solar radiation only contributes a small offset to the more prominent $1/r^2$ profile of the received microwave power. The no-return radius, on the other hand, is greatly affected by the presence of solar power harvesting. At large distances from the transmitter, received microwave power is negligible, and so the aircraft must rely

Table 3 Optimization parameters

Aircraft and mission parameters:			
AR	Wing aspect ratio	{1, 2.5, 5, 10, 20, 50}	
	Wing shape	{Rectangular, elliptic, bulbous}	
W_{pay}	Payload weight	2	kg
h	Altitude	1000	m
Cost functions:			
min P_{req}	Power required		W
max R	Range		m
max r_{eq}	Equilibrium power radius		m
max r_{nr}	No-return radius		m
Constraints:			
α	Angle of attack	$0 \le \alpha \le 15$	deg
$\frac{W_{\text{struct}}}{W_0}$	Structural weight fraction	$\frac{W_{\text{struct}}}{W_0} \ge 0.6$	
V	Cruise velocity	$V \ge 10.24$	m/s

Table 4 Minimal power configuration parameters

Aircraft and flight parameters:			
AR	Wing aspect ratio	10	
	Wing shape	Rectangular	
b	Wing span	3.81	m
W_0	Gross weight	13.92	kg
$\frac{W_{\text{struct}}}{W_0}$	Structural weight fraction	0.60	
S	Wing planform area	1.45	m^2
V	Cruise velocity	10.5	m/s
α	Angle of attack	13.9	deg
C_L	Lift coefficient	1.155	
W_0/S	Wing loading	9.6	kg/m^2
Performance metrics:			
P_{req}	Required power	242.7	W
R	Range	49.9	km
r_{eq}	Equilibrium power radius (with solar)	5.05	km
r_{eq}	Equilibrium power radius (without solar)	3.98	km
r_{nr}	No-return radius (with solar)	71.8	km
r_{nr}	No-return radius (without solar)	31.8	km

on solar power to extend its range. The range of the aircraft in the traditional sense [Eq. (15)] is actually smaller than the no-return radius for the case with solar power harvesting. This indicates the significant impact power harvesting has on this performance metric.

The loitering time for the aircraft as a function of distance from the transmitter is plotted in Fig. 5. For both the with- and without-solar cases, the trends can be divided into three distinct regions. The first region is the area around the transmitter in which the loiter time is infinite; this is indicated by a vertical asymptote at the equilibrium power radius. In this region, the power harvested is greater than the power required for flight, resulting in a net power gain. The second region begins just outside the equilibrium power radius, where the power received from microwave transmission is still significant. The loiter time in this region is greatly affected by the power received from the transmitter and decays in a manner similar to the $1/r^2$ power profile of the microwave radiation. The third region includes all distances where the power required for cruise is much larger than the power harvested by the rectenna. In this region, the loiter time decays approximately linearly with distance, which is similar to the case for a non-power-harvesting aircraft with a fixed fuel supply. Finally, the loiter time reaches 0 at the no-return radius.

These regions are also depicted in the surveillance envelope shown in Fig. 6, where the distances in Fig. 5 are graphed as radii from the origin where the transmitter is located. This plot shows five areas with fundamentally different characteristics. Region I is bounded by the equilibrium power radius; it represents the area in which the aircraft can loiter indefinitely. As stated previously, in this area the power harvested is greater than the power required for flight. Region II is fully, radially observable: in this area the plane can circle the transmitter at least once. The stored energy is continually decreasing in this region, and the plane eventually requires a return to region I to recharge. Region III represents the area where the plane can only fly a partial arc before returning to region I. Here, the aircraft flies directly out to a specified radius, sweeps out an arc symmetric to the positive y axis, and then returns to region I. The decrease in stored energy during flight in this region is depicted qualitatively in Fig. 4. The length of this arc decreases from 360 deg to 0 at the no-return radius, because at this radius, the aircraft only has enough energy to fly out and directly back again. Region IV represents an area that cannot be flown through from an arbitrary exit point from region I. Because the direction along which region III is aligned is arbitrary, it can be rotated to cover any sector of region IV. However, if multiple sectors of region IV are to be surveyed, then the aircraft must return to region I to recharge its batteries. Finally, region V covers the area outside the no-return radius. If the aircraft flies into this region, it will run out of stored energy (and, hence, thrust) before it makes it back to region I. It should be noted, however, that this plot is generated under the assumption of constant altitude flight; any altitude the aircraft may sacrifice can extend these radii and enlarge the entire plot.

B. Performance Sensitivity to Sizing and Angle of Attack

The previous section describes the surveillance capabilities for a single fuel-less aircraft design. In this section, the changes in the various performance metrics listed in Table 4 with respect to flight condition and aircraft sizing are analyzed. Again, a rectangular wing of aspect ratio 10 is chosen, but the scale and cruise angle of attack are allowed to vary, within the constraints listed in Table 3. The results of these variations within the feasible design space are shown in Fig. 7 for the case of no solar energy harvesting. (Solar energy harvesting is

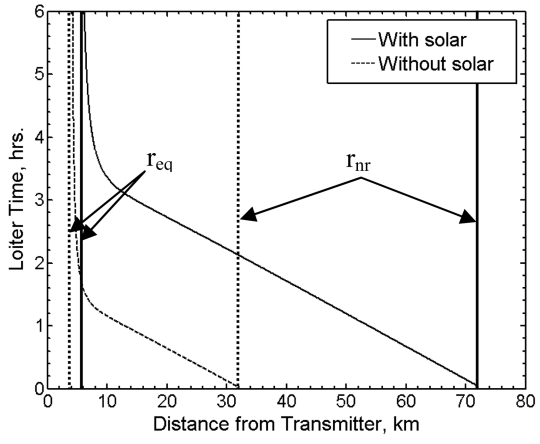

Fig. 5 Loiter time vs distance from transmitter.

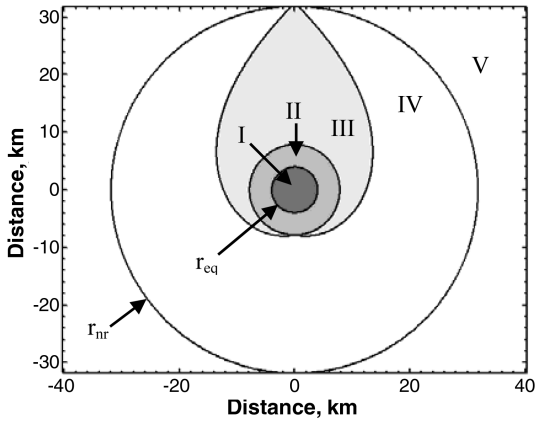

Fig. 6 Surveillance envelope, indicating regions of coverage.

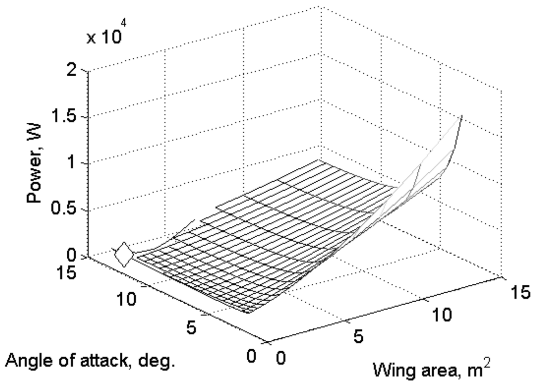

a)

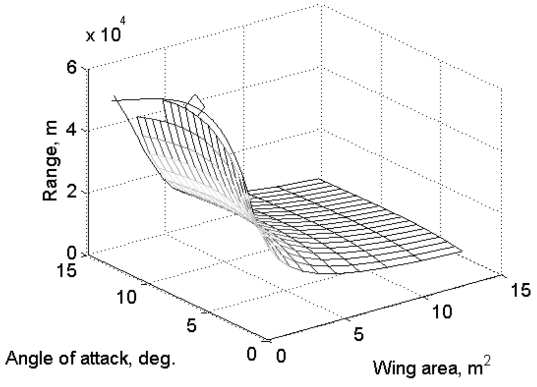

b)

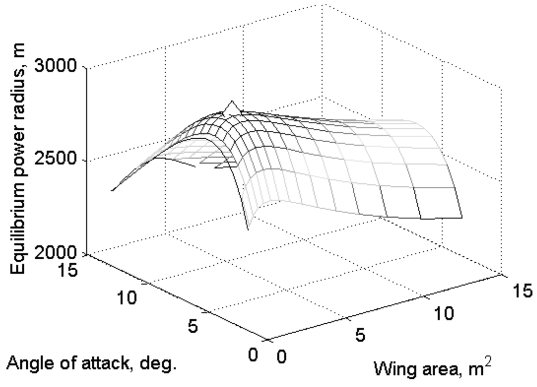

c)

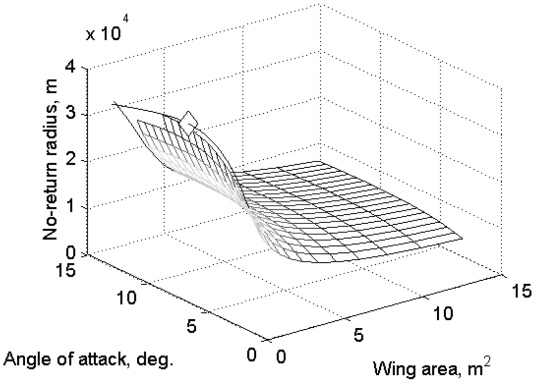

d)

Fig. 7 Variations in several performance metrics over the feasible design space, without solar energy harvesting: a) P_{req}, b) R, c) r_{eq},and d) r_{nr}. Optimum configurations are indicated by ⋄.

added in below.) The two design parameters, trim angle of attack and wing area, are plotted along the horizontal axes, and the performance metric is plotted along the vertical. The optimum parameters and the constraint boundaries are also indicated on each plot.

Figure 7a indicates that the minimum required power configuration has a small wing area and flies at a high angle of attack, which leads to a small cruise velocity. Both of these factors contribute to low drag while still maintaining the required lift for straight-and-level flight. Although it is difficult to see in the plot, power increases again as the wing area decreases past 1.45 m^2 because the aircraft must fly much faster to carry the required payload. Even smaller configurations fail to meet the minimum structural weight fraction requirement. Moderately sized aircraft (2–4 m^2) fail to meet the minimum flight speed requirement at high angles of attack. Figure 7b indicates that the maximum range occurs with a small aircraft at a moderate angle of attack. This provides the balance between high-speed flight and low power consumption as governed by Eq. (15). The range decreases rapidly as size increases due to the rise in required power. Figure 7c depicts variations in equilibrium power radius. As mentioned previously, this metric is maximized at low angles of attack and low values of S/P_{req}. This is indicated in Fig. 7c, where the maximum r_{eq} is found at low angles of attack and moderate wing area, where there is a balance between area and power required. Flight at higher angles of attack reduces the received power when flying away from the transmitter, as governed by Eq. (10). Figure 7d shows that the no-return radius is almost exactly proportional to range, as predicted. This indicates that wing area in and of itself is not important because microwave energy is insignificant at large distances from the transmitter. Thus, the trends in Fig. 7d closely follow those of Fig. 7b.

When solar energy harvesting is included, the required power and the range remain unchanged; however, the equilibrium power radius and no-return radius are affected, as shown in Figs. 8a and 8b.

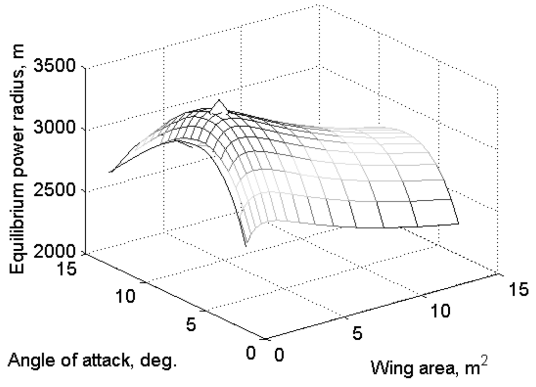

a)

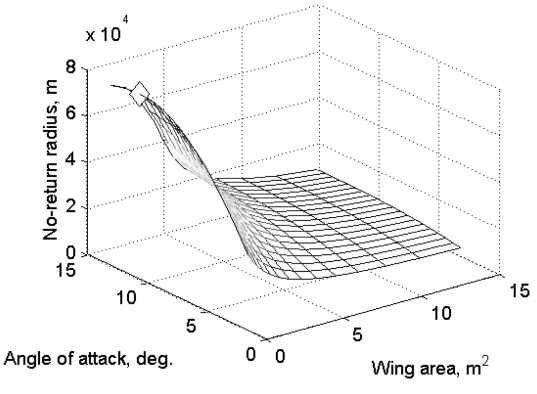

b)

Fig. 8 Variations in several performance metrics over the feasible design space, with solar energy harvesting: a) r_{eq}, and b) r_{nr}. Optimum configurations are indicated by ⋄.

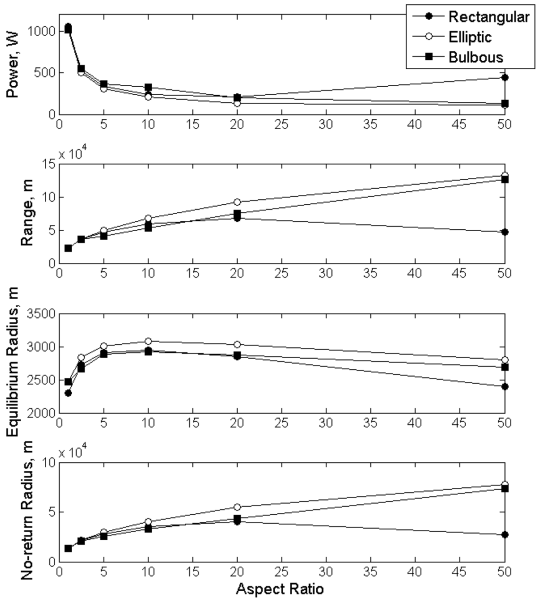

Fig. 9 Optimum performance vs aspect ratio for three wing shapes.

[Compare to Figs. 7c and 7d.] The equilibrium power radius' trends are similar, but the magnitude is slightly increased. As previously discussed, this is because the harvested microwave energy is dominant at these distances. On the other hand, the no-return radius is greatly increased by the effects of solar energy, as seen previously in Fig. 5. The trends shown in Fig. 8b are more closely affected by the required power more than the wing area itself. Thus, when solar power dominates, which is the case in the no-return radius calculation, the most important factor in maximizing the no-return radius is minimizing the required power for flight.

C. Wing Shape Sensitivity

The four metrics presented in Fig. 7 are now plotted against the aspect ratio for the three wing shapes listed in Table 3, without solar energy harvesting. The optimum values for each metric, aspect ratio, and wing shape are presented in Fig. 9.

These plots indicate that at low aspect ratios, all three wing shapes perform comparably, albeit poorly. At these aspect ratios, significant downwash across the wings occludes any geometrical advantage. At moderate aspect ratios, the large downwash over the inboard section of the bulbous wing degrades its performance by lowering its lift-to-drag ratio at every angle of attack, compared to the other two wing shapes. However, at high aspect ratios, the bulbous wing behaves as

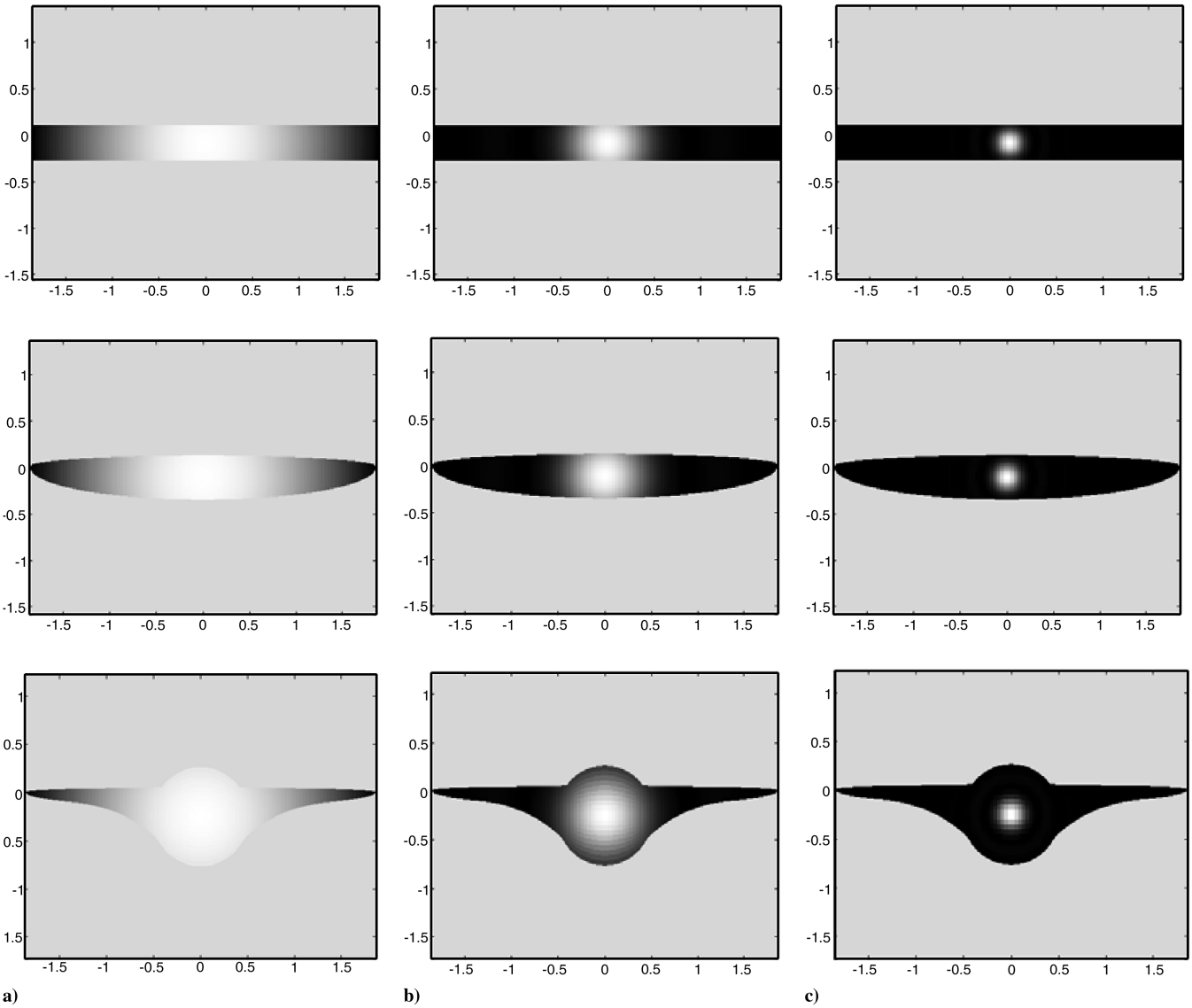

a) b) c)

Fig. 10 Received microwave power intensity distribution for aa) $G_{tr} = 60$ dB, b) $G_{tr} = 70$ dB, and c) $G_{tr} = 80$ dB.

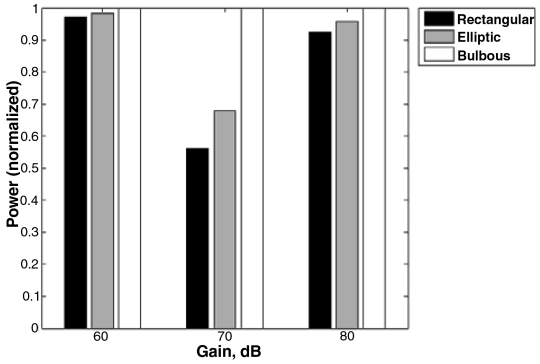

Fig. 11 Power consumption as a function of wing shape and transmitter gain.

an elliptic wing and outperforms the rectangular wing. The degradation of the rectangular wing's performance is mainly attributed to its large structural weight penalty (due to the extra structure needed to support a relatively heavy cantilever).

Although the bulbous wing cannot outperform the elliptic wing aerodynamically, it is better suited to receive microwave power. This can be clearly seen in Fig. 10, where the distribution of received power intensity is plotted for several values of transmitter gain. This gain is varied by adjusting the radius of the dish.

These plots indicate the received power distribution over the wing planform when the aircraft is flying directly overhead of the transmitter. In this situation, the distribution is circular, with the center of the beam aimed at the center of the root chord. At low gain, most of the planform receives comparable power due to the low directivity of the transmitter. Similarly, at high gain, the beam is extremely focused at this range, and only the center of the wing receives appreciable power. However, at gains in between these two cases, the shape of the bulbous wing become significant, because its size is comparable to the width of the beam. Thus, the geometry of the wing is only significant when the aircraft is properly sized to the transmitter. This conclusion is quite apparent in Fig. 11, where the integrated power over the planform is presented for each wing shape and normalized to the maximum value for each gain. Only in the $G_{\text{tr}} = 70$ dB is there a significant difference in the wing shapes' power reception.

IV. Conclusions

Microwave- and solar-powered aircraft present an extraordinary concept for aircraft design due to their potential for extremely long endurance flights. Moreover, both energy sources rely on the wing planform area for harvesting, and so they can be maximized by the same aircraft design. However, the coupling of aerodynamics and power harvesting capabilities adds an additional layer of complexity to the conceptual design process. It has been demonstrated in this study that aerodynamic performance and power harvesting performance cannot be designed independently. The minimum flight power configuration minimizes the power requirements of the transmitter; however, it does not maximize the area in which the aircraft can loiter indefinitely while harvesting energy. This disparity is shown to arise from the offsetting effects of increased wing area: added weight and added power harvesting surface. New performance metrics have been introduced, such as the equilibrium power radius and the no-return radius, that quantify the unique characteristics of these aircraft and illuminate the relative impact of aerodynamic and power harvesting performance on mission capability. Furthermore, these metrics indicate that the sizing and geometry of the aircraft must be designed simultaneously with the transmitter and matched to the mission and payload requirements to make the most efficient use of the aircraft's harvesting capabilities. This has been demonstrated by matching the beamwidth of the microwave transmission to the size and shape of the wing planform. Indeed, a mismatch of any of these aspects will lead to degraded performance. Nevertheless, despite these complications and caveats, the utility of a persistent airborne surveillance platform is undeniable.

Acknowledgment

This work is supported in part by the Intelligence Community (IC) Postdoctoral Research Fellowship Program, monitored by Jim Beckwith.

References

[1] Brown, W. C., "The History of Power Transmission by Radio Waves," *IEEE Transactions on Microwave Theory and Techniques*, Vol. 32, No. 9, 1984, pp. 1230–1242. doi:10.1109/TMTT.1984.1132833

[2] Klesh, A. T., and Kabamba, P. T., "Energy-Optimal Path Planning for Solar-Powered Aircraft in Level Flight," AIAA Paper 2007-6655, 2007.

[3] Brown, W. C., "Experiments Involving a Microwave Beam to Power and Position a Helicopter," *IEEE Transactions on Aerospace and Electronic Systems*, Vol. aes-5, No. 5, 1969, pp. 692–702. doi:10.1109/TAES.1969.309867

[4] DeLaurier, J., Gagnon, B., Wong, J., Williams, R., Hayball, C., and Advani, S., "Flying High with HALE: Progress Report," *Unmanned Systems*, Vol. 5, No. 3, 1987, pp. 25–46.

[5] Brown, W. C., "Rectenna Technology Program: Ultra Light 2.45 GHz Rectenna and 20 GHz Rectenna," NASA CR-179558, March 1987.

[6] Kim, J., Yang, S. Y., Song, K. D., Jones, S., and Choi, S. H., "Performance Characterization of Flexible Dipole Rectennas for Smart Actuator Use," *Smart Materials and Structures*, Vol. 15, No. 3, 2006, pp. 809–815. doi:10.1088/0964-1726/15/3/017

[7] Heyson, H. H., "Initial Feasibility Study of a Microwave-Powered Sailplane as a High-Altitude Observation Platform," NASA TM-78809, Dec. 1978.

[8] Turriziani, R. V., "Sensitivity Study for a Remotely Piloted Microwave-Powered Sailplane Used as a High-Altitude Observation Platform," NASA CR-159089, June 1979.

[9] Morris, C. E. K., "Parametric Study of Microwave-Powered High-Altitude Aircraft Platforms Designed for Linear Flight," NASA TM-1918, Nov. 1981.

[10] Morris, C. E. K., "Microwave-Powered, Unmanned, High-Altitude Airplanes," *Journal of Aircraft*, Vol. 21, No. 12, 1984, pp. 966–970. doi:10.2514/3.45070

[11] Sinko, J. W., "Circling Flight in Wind for HAPP Aircraft," SRI TN SED-716, Aug. 1978.

[12] Edwards, E. C., "An Algorithm for Autonomous Flight Control of Unmanned Stationkeeping Aircraft," M.Sc. Thesis, University of Toronto, Toronto, ON, Canada, 1990.

[13] Klesh, A. T., and Kabamba, P. T., "Energy-Optimal Path Planning for Solar-Powered Aircraft in Level Flight," AIAA Paper 2007-6655, 2007.

[14] Wickenheiser, A. M., and Garcia, E., "Multisource Power Harvesting for Fuel-Less Air Vehicles," *Proceedings of SPIE: International Society for Optical Engineering*, Vol. 6928, SPIE–International Society for Optical Engineering, Bellingham, WA, 2008.

[15] Edwards, E. C., and McKinney, W. D., "Performance Evaluation of the 12m SHARP Prototype," Aeronautical Design, Inc., Toronto, Ontario, Canada, March 1992.

[16] Raymer, D. P., "Initial Sizing," *Aircraft Design: Conceptual Approach*, 3rd ed., AIAA, Reston, VA, 1999, pp. 122–125.

[17] Wickenheiser, A., and Garcia, E., "Aerodynamic Modeling of Morphing Wings Using an Extended Lifting-Line Analysis," *Journal of Aircraft*, Vol. 44, No. 1, 2007, pp. 10–16. doi:10.2514/1.18323

[18] Prandtl, L., "Applications of Modern Hydrodynamics to Aeronautics," NACA TR-116, 1923.

[19] Raymer, D. P., "Aerodynamics," *Aircraft Design: Conceptual Approach*, 3rd ed., AIAA, Reston, 1999, pp. 340–346.

[20] Raymer, D. P., "Weights," *Aircraft Design: Conceptual Approach*, 3rd ed., AIAA, Reston, 1999, p. 476.

[21] "Brushless Outrunners," http://www.bphobbies.com/view.asp?id=A1190096 [retrieved 3 March 2008].

[22] Ward, J., Ramanathan, K., Hasoon, F., Coutts, T., Keane, J., Moriarty, T., and Noufi, R., "Cu(In,Ga) Se_2 Thin-Film Concentrator Solar Cells," NREL, NREL/CP-520-31144, Oct. 2001.

[23] Johnson, D. L., "Terrestrial Environment (Climatic) Criteria Guidelines for Use in Aerospace Vehicle Development," NASA TM-4511,

Aug. 1993.
[24] Ren, Y., and Chang, K., "5.8-GHz Circularly Polarized Dual-Diode Rectenna and Rectenna Array for Microwave Power Transmission," *IEEE Transactions on Microwave Theory and Techniques*, Vol. 54, No. 4, 2006, pp. 1495–1502. doi:10.1109/TMTT.2006.871362
[25] Johnson, R. C., and Henry, J. (eds.), *Antenna Engineering Handbook*, McGraw–Hill, New York, 1984.
[26] Raymer, D. P., "Sizing from a Conceptual Sketch," *Aircraft Design: Conceptual Approach*, 3rd ed., AIAA, Reston, 1999, pp. 16–17.
[27] Powell, M. J. D., "A Fast Algorithm for Nonlinearly Constrained Optimization Calculations," *Numerical Analysis*, edited by G. A. Watson, Vol. 630, Lecture Notes in Mathematics, Springer–Verlag, Berlin, 1978, pp. 144–157.
[28] Dormand, J. R., and Prince, P. J., "A Family of Embedded Runge-Kutta Formulae," *Journal of Computational and Applied Mathematics*, Vol. 6, No. 1, 1980, pp. 19–26. doi:10.1016/0771-050X(80)90013-3